PAPER

Check for updates

Selective enhancement of upconversion luminescence for enhanced ratiometric sensing

Kyuyoung Bae,[a] Bo Xu,[b] Ananda Das,[b] Connor Wolenski,[a] Eric Rappeport[a] and Wounjhang Park [ID] *[ac]

Lanthanide-doped upconversion nanoparticles (UCNPs) have attracted widespread interest in bioimaging and sensing due to their photostability, low excitation energy, and good tissue penetration. Plasmonic nanostructures, on the other hand, can enhance the luminescence of UCNPs by concentrating electric fields into a nanoscale volume. While the enhanced luminescence intensity is in principle beneficial to sensing, intensity-based sensing has limitations in absolute measurements. This deficiency can be overcome by employing ratiometric sensing in which intensity ratio, rather than intensity itself, is used to quantitatively determine the presence of analytes. The ratiometric sensing is advantageous because the intensity ratio is much less sensitive to the variations in the environment and the number of probe materials in the sensing volume. Here, we demonstrate a plasmonic nanostructure with upconversion nanoparticles for an enhanced ratiometric sensing platform. The plasmonic nanostructure is composed of UCNPs, an indium tin oxide (ITO) spacer layer and an Au nanodisk. The nanostructure is designed such that the plasmon resonance selectively enhances the red luminescence of $NaYGdF_4$:Yb^{3+}, Er^{3+} UCNPs while leaving the green luminescence unaffected, thereby increasing the dynamic range and achievable sensitivity of the red-to-green (R/G) intensity ratio. We observed a 4-fold enhancement in the R/G ratio and also a drastic reduction in the signal uncertainty. This work advances our knowledge of the optical interaction between UCNPs and plasmonic nanostructures and also provides a foundation for improved ratiometric sensing in biomedical applications.

1. Introduction

Upconversion luminescence has been attracting much attention for a variety of applications including photovoltaics[1,2] and biological imaging.[3,4] Upconversion nanoparticles (UCNPs) activated with lanthanide ions are especially useful for biomedical applications as they have excellent photostability, narrow emissions bands, and low cytotoxicity. Moreover, the use of near-infrared (NIR) excitation has numerous advantages compared to UV and visible light. The UV and visible light, which are used in conventional fluorescence imaging, often excites background fluorescence from the surrounding tissue. In contrast, the NIR light does not excite background fluorescence and penetrates deep into tissues with minimal damages thanks to the high tissue transparency. Two-photon fluorescence microscopy takes advantage of the NIR excitation but UCNPs exhibit many orders of magnitude higher efficiency than the two-photon dyes or proteins. As a result, UCNP-based

imaging provides high contrast against the background with low excitation power density.

Metallic nanostructures supporting surface plasmon resonances exhibit strongly enhanced local electric fields in the vicinity of a metal surface.[5] The high local fields lead to enhanced light-matter interaction resulting in stronger light scattering, absorption, and emission. In particular, plasmon enhancement of luminescence is of great interest to applications in imaging[6–9] and sensing.[10–14] Plasmon enhancement of luminescence, often referred to as the Purcell effect, arises from the increased photon density of states due to the plasmon resonance.[15,16] The actual enhancement factor is determined by the combination of the Purcell effect and the unavoidable quenching by metals. In any case, since luminescence is a linear process, the plasmon-enhanced luminescence intensity is linearly proportional to the local intensity enhancement factor, which is determined by the details of the nanostructure geometry and materials used.[17]

While enhanced luminescence intensity can generally enhance the sensing capability, intensity-based sensing faces a fundamental challenge in absolute measurements. Intensity-based sensing is capable of quantitative measurements only when the full information on the luminescent probes, such as the number of probes within the sensing volume, is known.

[a]Department of Electrical, Computer and Energy Engineering, University of Colorado Boulder, 425 UCB, Boulder, CO 80309, USA

[b]Department of Physics, University of Colorado Boulder, 425 UCB, Boulder, CO 80309, USA

[c]Materials Science & Engineering Program, University of Colorado Boulder, 425 UCB, Boulder, CO 80309, USA. E-mail: won.park@colorado.edu

This is possible when the samples can be taken into a well-calibrated apparatus.[18,19] However, when the samples need to be measured in their natural states, it is generally difficult to control the delivery of luminescent probes, and the number of probes within the sensing volume is often unknown. Many biosensing experiments, whether *in vitro* or *in vivo*, fall in this category.[20] In these cases, intensity-based sensing can only give relative changes between samples. To make matters worse, luminescent probes may change their quantum efficiency due to the interaction with the environment. For example, a probe placed near a strongly absorbing material may exhibit significant luminescence quenching. For absolute measurements, a rigorous calibration process, which is often extremely difficult to carry out, is necessary.

A simple yet powerful technique to overcome this fundamental difficulty is to employ ratiometric sensing. In this method, a luminescent probe with two or more emission wavelengths is used. Among the multiple emission lines, one is affected by the presence of the analyte, while another remains unchanged. The luminescence intensity unaffected by the analyte serves as the reference against which the analyte-sensitive luminescence intensity is calibrated. The intensity ratio does not depend on the number of probe molecules or nanoparticles in the sensing volume. Even in the presence of interaction with the environment that may affect the quantum efficiency, the ratio will be preserved as long as the interaction has a weak wavelength dependence and thus affect the two intensities in the same way.

UCNP is an excellent probe for ratiometric sensing since they exhibit multiple narrow-line luminescence in the visible and NIR region.[21–26] Adding the benefits of ratiometric sensing to the well-established advantages of plasmon enhancement of upconversion would lead to a powerful sensing platform. In particular, the highly selective enhancement of one luminescence colour should provide greater sensitivity and wider dynamic range. In this paper, we present a prototypical plasmonic nanostructure with UCNPs as an effective ratiometric sensing platform. The plasmonic nanostructure is composed of UCNPs and an Au nanodisk with an indium tin oxide (ITO) spacer layer. We study the red-to-green (R/G) intensity ratios for different spacer layer thicknesses to observe how the plasmonic effect changes and confirm the experimental results with numerical simulations. The results show that ratiometric sensing greatly reduces the uncertainty in the signal while the plasmonic structure expands the sensitivity and dynamic range of ratiometric sensing.

2. Experimental section

2.1 Upconversion nanoparticles synthesis

$NaY_{0.55}Gd_{0.25}F_4$:$Yb_{0.18}Er_{0.02}$ upconversion nanoparticles were synthesized following the well-established co-precipitation method (Fig. 2(a)).[27] Gd ions were introduced to control the nanoparticle diameter[28–30] while the relative amount of surfactant influenced the nanoparticle aspect ratio.[31] Briefly, YCl_3 (43.0 mg), $GdCl_3$ (26.4 mg), $YbCl_3$ (20.1 mg), and $ErCl_3$ (2.2 mg) were mixed with oleic acid (3 mL) and 1-octadecene (7 mL) inside of a 100 mL three-neck round-bottom flask containing a magnetic stir bar and thermocouple. While stirring on a hot
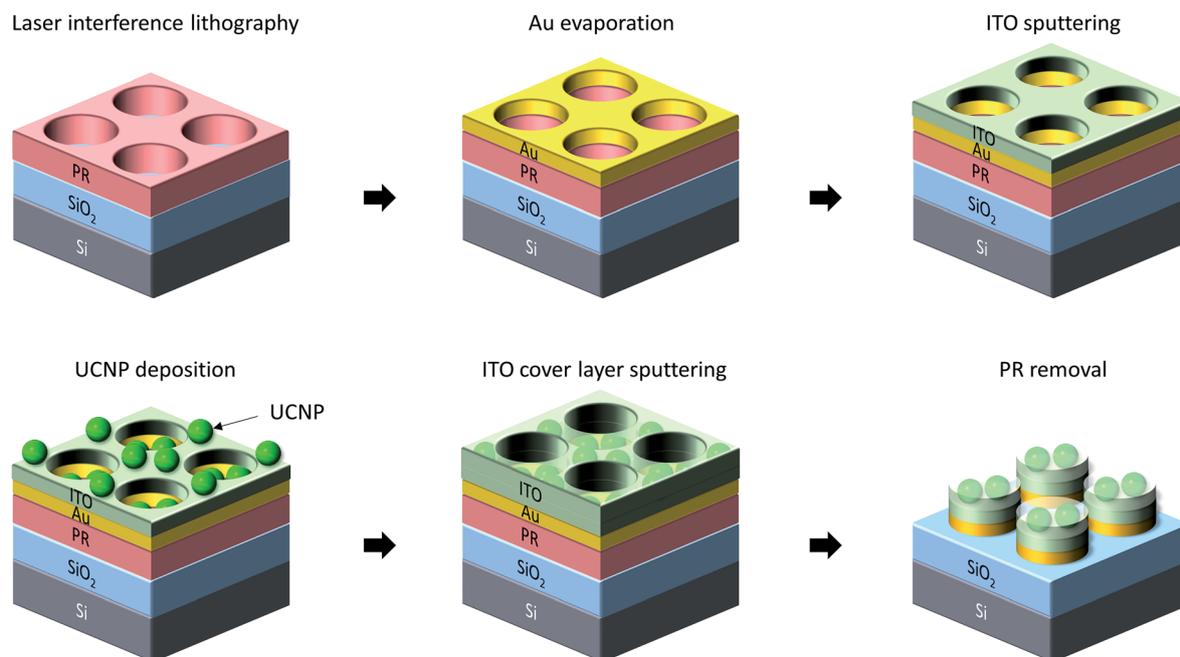
Fig. 1 The fabrication process for the plasmonic ratiometric sensing platform. Laser interference lithography generates hole arrays on the spun photoresist. A 15 nm Au layer is then thermally evaporated, and an ITO thin film is sputtered as a spacer layer. The UCNPs are deposited by a tape method. The concentration of spread UCNP solution is adjusted so that the UCNPs in the holes become monolayer. An additional ITO cover layer of 10 nm is deposited to UCNPs from being lost during the following PR removal process. Finally, the photoresist is removed, and then the plasmonic nanostructures remain on top of the SiO_2 substrate.
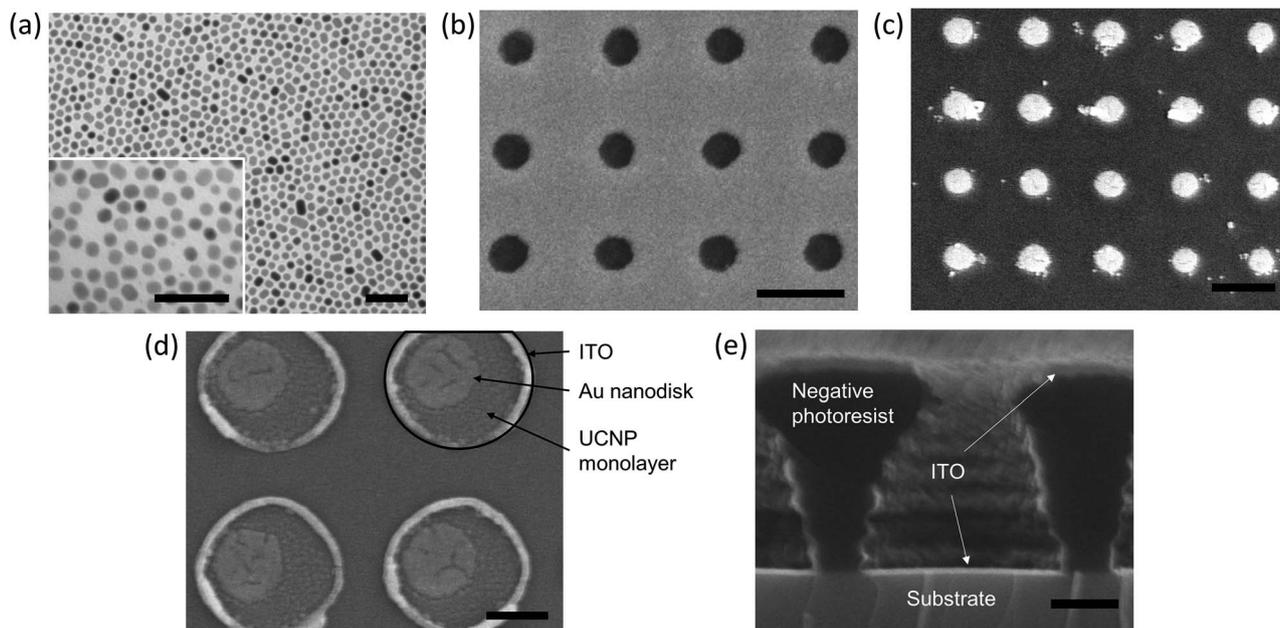
Fig. 2 TEM and SEM images of plasmonic nanostructures. (a) TEM image of synthesized UCNPs. The inset shows the high magnification image of the UCNPs. (b) Nanohole array after LIL and Au deposition before the photoresist layer was lifted off. (c) Au nanodisks and UCNPs without a spacer layer. A few UCNPs on the substrate are due to the PR removal process, but many UCNPs are on the Au nanodisks. (d) Au nanodisks and UCNPs with ITO spacer layer. The final Au nanodisk size is 230 nm in diameter with a period of 600 nm for both (b) and (c). (e) Cross-section image of ITO film with the photoresist. The scale bar: (a, inset) 100 nm, (b and c) 500 nm, and (d and e) 200 nm.

plate, the mixture was heated to 160 °C, held at this temperature for 10 minutes, and then cooled down to room temperature to form a homogenous solution. Meanwhile, NaOH (40.0 mg) and NH_4F (59.3 mg) were dissolved in methanol (20 mL). The methanol solution was then added dropwise using a glass pipette to the room temperature rare-earth mixture and stirred for thirty minutes. Under a gentle flow of argon, the solution was heated to 100 °C and purged for 25 minutes. Next, the reaction vessel was sealed, transferred to a round bottom heater, and heated to 300 °C. After 1 hour, the solution was cooled naturally to room temperature and washed by adding 200 proof ethanol and centrifuging at 7000 rpm for 10 minutes. The nanoparticles were precipitated at the bottom of the tube, and the supernatant was discarded. This process was repeated three times. Finally, the nanoparticles were dried in an oven at 60 °C for 12 hours before being dispersed in toluene.

2.2 UCNP-ITO-Au nanodisk fabrication

The fabrication process for the plasmonic nanostructure is schematically shown in Fig. 1. First, we spin-coated a photoresist (NR9-1000P, Futurrex, Inc.) on a 6 μm thick thermally grown silica substrate. Laser interference lithography (LIL) was performed using a Lloyd mirror setup to obtain a hole array with a period of 600 nm. We then deposited an Au layer of 15 nm by thermal evaporation. To study the effect of a spacer layer, an ITO thin film was sputtered on top of the Au nanodisks. ITO was chosen for the spacer layer because it is transparent in the visible range and easily deposited by the sputtering process. Next, we deposited UCNPs by drying the UCNP solution in a confinement cell. This

process has been used to obtain uniform UCNP layers in our previous works.[8,32] In this work, the UCNP concentration was adjusted to 250 μg mL^{-1}, and the solvent was evaporated at 60 °C to obtain a uniform monolayer. To ensure UCNPs stay affixed to the nanostructure, we sputtered a 10 nm thick ITO overlayer on top of the UCNP layer. Finally, the photoresist layer was removed by immersing the sample in acetone with sonication.

Fig. 2(b) shows the nanohole array produced by LIL on top of which an Au layer is evaporated. The image shows a uniform array of nanoholes with a diameter of 230 nm. Fig. 2(c) shows UCNP-coated Au nanodisks without an ITO spacer layer. The Au nanodisk diameter is 230 nm, the same as in Fig. 2(b). The Au nanodisks with ITO spacer layers are shown in Fig. 2(d). It is noted that the sputtered ITO nanodisks are larger than the underlying Au nanodisks. This is due to the shape of the nanoholes fabricated by LIL. As shown in Fig. 2(e), the nanohole pattern produced by LIL has a vertical profile such that the opening at the top surface is smaller than the void at the bottom. This is a typical profile for a negative photoresist.[33] Since thermal evaporation is a directional deposition technique, the Au nanodisk size is determined by the size of the holes at the top surface of the photoresist. In contrast, the ITO diameter is determined by the size of the opening at the bottom as the sputtering is an isotropic deposition process. It is noted that Fig. 2(d) also shows that the UCNPs are uniformly deposited.

The lithographic fabrication procedure outlined in Fig. 1 allows us to achieve highly uniform nanostructures that can be easily dispersed into water for biosensing applications. The high uniformity results in a consistent, narrowband resonance exhibited by all the nanostructures. The well-defined resonance

with minimal inhomogeneous broadening is critical for ratiometric sensing applications as it lets us target the red emission line of the UCNPs without affecting the green wavelengths. This is in stark contrast to other reported Purcell enhancement values where, due to the nonuniformity introduced from the fabrication techniques involved, the plasmonic nanostructure resonance bleeds into green wavelengths and enhances them as well.[34–37] As we will discuss in the next section, our plasmonic nanostructure is able to achieve comparable levels of red enhancement to other reported values while leaving the green emission unchanged thus demonstrating the potential for use as a ratiometric sensor with enhanced dynamic range and sensitivity.

3.   Results and discussion

We simulated the plasmonic nanostructure to investigate the Au nanodisk's Purcell effect using the commercial finite-difference time-domain (FDTD) simulation tool, Lumerical. As shown in Fig. 3(a), we placed the Au nanodisk on the SiO$_2$ substrate and the ITO and UCNP layers on the top of the Au nanodisk. We also included a 10 nm-thick ITO overlayer on top of the UCNP layer in all simulations. The Purcell factor was calculated by dividing the power emitted by a dipole source with the plasmonic structure by the power emitted by the same dipole in free space. To accurately represent the experimental condition where UCNPs are deposited uniformly over the nanostructure, we averaged the Purcell factors over polarizations and also over the volume of the region designated as UCNP layer in Fig. 3(a). As shown later, in the fabricated samples, the ITO and UCNP regions are larger in diameter than the Au nanodisk. However, the presence of UCNPs outside the Au nanodisk makes only negligible changes because the main contributions are from the UCNPs strongly coupled with the plasmon resonance of the Au nanodisk.

Fig. 3(b) shows the simulated Purcell factors with various spacer thicknesses from 0 to 40 nm. The Au nanodisk, ITO, and UCNP layer diameters are 230 nm, and the Au nanodisk and UCNP layer thicknesses are 15 nm and 18 nm, respectively. The Au nanodisk's diameter and thickness are designed to have the main resonance at 654 nm with an ITO spacer of 10 nm. The shoulder features at the shorter wavelengths are due to a higher order plasmon modes and do not affect our study. With no spacer layer, the plasmonic structure exhibits strong quenching, and thus, the Purcell enhancement is weak. Also, the plasmonic resonance is shifted to 610 nm, making the R/G ratio enhancement smaller than the plasmonic structure with a 10 nm ITO spacer. With the addition of the ITO space layer, the Purcell factor for the red wavelength jumps to ~4. It gradually decreases as the spacer layer thickness is increased because the local field enhancement is weaker and also because the plasmon resonance red-shifts away from the luminescence wavelength. The red-shift is due to the increase in the effective refractive index near the dipole[38] while the decrease of Purcell factor is the result of decreasing field enhancement with increasing distance from the metal surface.[39] It should be noted that the Purcell factor for the green wavelength remains nearly unchanged. We therefore control the R/G intensity ratio by controlling the Purcell effect with spacer layer thickness.

Fig. 3(c) shows the ratio of Purcell factor at 645 and 556.4 nm, which are the wavelengths of red and green emission lines of the Er^{3+} ion. Following the behavior of Purcell factors in Fig. 3(b), the R/G ratio is small without a spacer layer and jumps to 3.6 with a 10 nm thick spacer layer. With further increase in spacer layer thickness, the ratio gradually decreases. In the proposed sensing scheme, the enhanced red luminescence is to be used as the signal, while the unaffected green luminescence is to serve as the reference. By selectively enhancing red luminescence only, the plasmon enhancement effect of red luminescence is directly translated to the R/G intensity ratio. Thus, the R/G ratio based sensing now enjoys the same benefits of plasmon enhancement, leading to higher sensitivity and larger dynamic range.
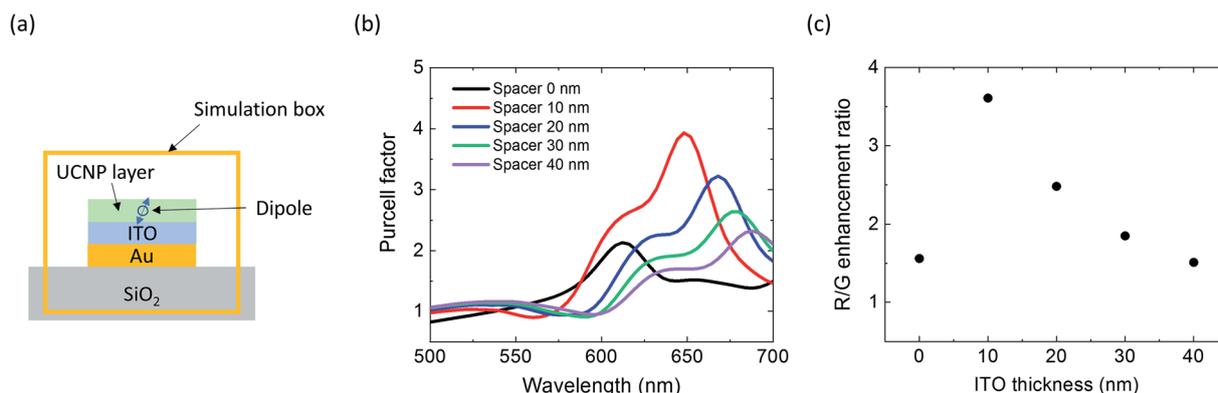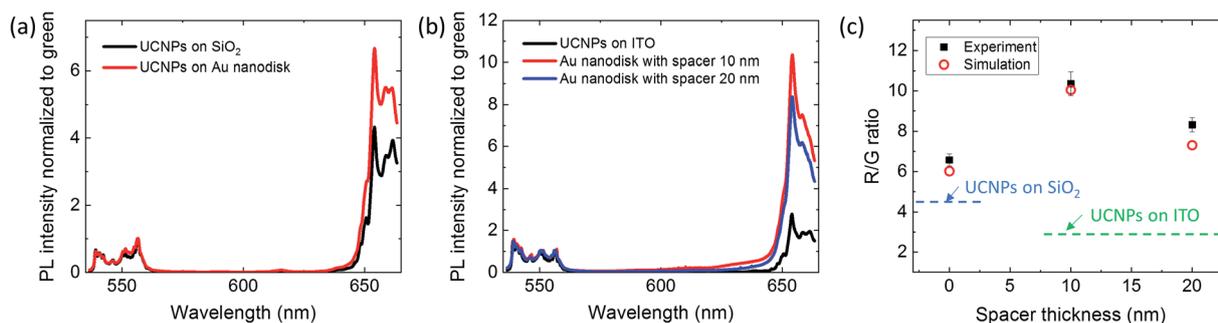

Fig. 3 Simulation of the plasmonic nanostructure. (a) The schematic of the Purcell factor simulation. We also included a 10 nm-thick ITO overlayer on top of the UCNP layer in all simulations. A dipole source is placed in the UCNP layer. The Purcell factor is calculated by dividing the power emitted by a dipole source with the plasmonic structure by the power emitted by the dipole without the structure. The Purcell factors are averaged for x, y, and z polarization and the various dipole positions from the center to the edge of the UCNP layer. (b) Purcell factor spectra of the Au nanodisk and UCNP layer with different ITO spacer thicknesses. The Au nanodisk size is 230 nm in diameter and 15 nm in thickness, and the period of the Au nanodisk array is 600 nm. The UCNP layer thickness is 18 nm. (c) The red (654 nm) to green (556.4 nm) ratio of the calculated Purcell factors. The red to green ratio decreases as the ITO thickness increases due to the resonance shift and plasmonic effect reduction.

Fig. 4 Experimental PL of the plasmonic nanostructure. (a) PL spectra of the UCNPs on SiO_2 (black line) and on Au nanodisk without any spacer layer (red line). (b) PL intensities of the UCNPs on 20 nm ITO layer on SiO_2, and PL intensities with Au nanodisks and ITO spacer layer. The spectra are normalized to 556.4 nm for (a) and (b). (c) The red (654 nm) to green (556.4 nm) ratio of the measured PL intensities and simulated Purcell factors. The Purcell factors are weighted to the measured PL intensities without the Au nanodisks. The Purcell factors without (0 nm) and with ITO spacer layers (10 and 20 nm) are weighted to PL of UCNPs on SiO_2 and of UCNPs on 20 nm ITO layer on SiO_2, respectively, due to the different UCNPs' PL depending on the presence of the ITO layer.

The PL spectroscopy was performed using a confocal laser scanning microscope coupled with a spectrometer (Renishaw InVia). The samples were excited with a 980 nm wavelength laser (CrystaLaser DL980-500), and the emission from the UCNPs was collected by a silicon CCD detector. The excitation laser power was 33 mW. Fig. 4 shows the measurement results of the plasmonic nanostructure. The measured PL results are normalized to 556.4 nm to clearly show the changes in the R/G ratio.

The measured PL spectra show the anticipated R/G ratio enhancement by the Au nanodisks. The black line in Fig. 4(a) is the PL spectrum of the UCNPs on a SiO_2 substrate without Au

nanodisks, exhibiting an R/G ratio of 4.4. The UCNPs on Au nanodisk without any spacer layer showed an R/G ratio of 6.6, reflecting the plasmon enhancement of red PL emission due to the Au nanodisk. The measured enhancement factor for the R/G ratio of 1.5 agrees well with the simulation result of 1.6 shown in Fig. 3(c). Fig. 4(b) shows the PL intensities of UCNPs on the ITO layer with and without the Au nanodisks. The R/G ratio of UCNPs on a 20 nm thick ITO layer was smaller than that of UCNPs on the SiO_2 substrate because sputtered ITO has stronger absorption in the red wavelengths than in the green.[40] However, the addition of Au nanodisks with plasmon resonance at 654 nm significantly increased the red luminescence intensity, resulting in R/G ratios of 10.4 and 8.3 for ITO spacer layer thicknesses of 10 nm and 20 nm, respectively. The R/G ratio with a 20 nm ITO layer is lower than that with a 10 nm ITO layer because the plasmonic resonance with the 20 nm ITO layer is both weaker and red-shifted away from the emission wavelength (see Fig. 3(b)), resulting in lower PL enhancement at 654 nm. There should also be a small contribution from greater ITO absorption in the red due to the larger thickness. We note that thermal quenching by local heating of Au nanodisks is not an issue because UCNP shows thermal enhancement of luminescence intensity with increasing temperature up to 200 °C and the expected temperature increase under typical experimental conditions is much smaller than that.[41]

We plotted the R/G ratios calculated from the simulated Purcell factors together with the measured R/G ratios in Fig. 4(c). The simulated R/G ratios were calculated by multiplying the simulated Purcell factors to the measured PL intensities of the reference samples. More specifically, for the 0-distance case, we used the UCNPs on a SiO_2 substrate as the reference for both measurements and simulations. For the samples with 10 and 20 nm thick ITO spacer layers, UCNPs deposited on the same thickness ITO layer on SiO_2 substrate were used as the reference in both simulations and experiments. Fig. 4(c) shows an excellent agreement between the experimental results and the predicted values from simulations.

To further confirm the observed enhancement of the R/G ratio is due to the plasmon resonance of properly designed Au
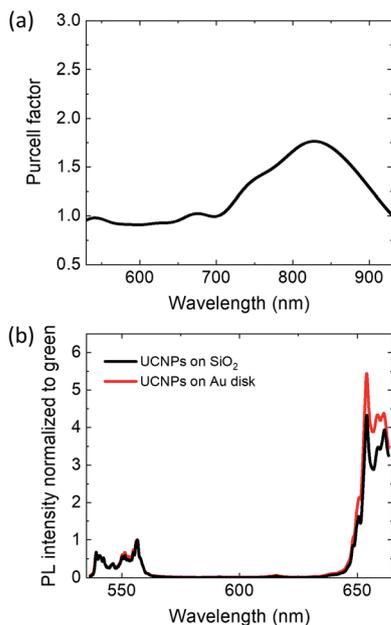
Fig. 5 Simulation and measurement spectra of the non-resonant Au disk with 190 nm in diameter and 30 nm in thickness. (a) Simulated Purcell factor of the Au disk. The plasmonic resonance is at 810 nm, and no resonances in red and green emission lines. (b) Experimental PL of UCNPs on SiO_2 and the Au disk on SiO_2 substrate.
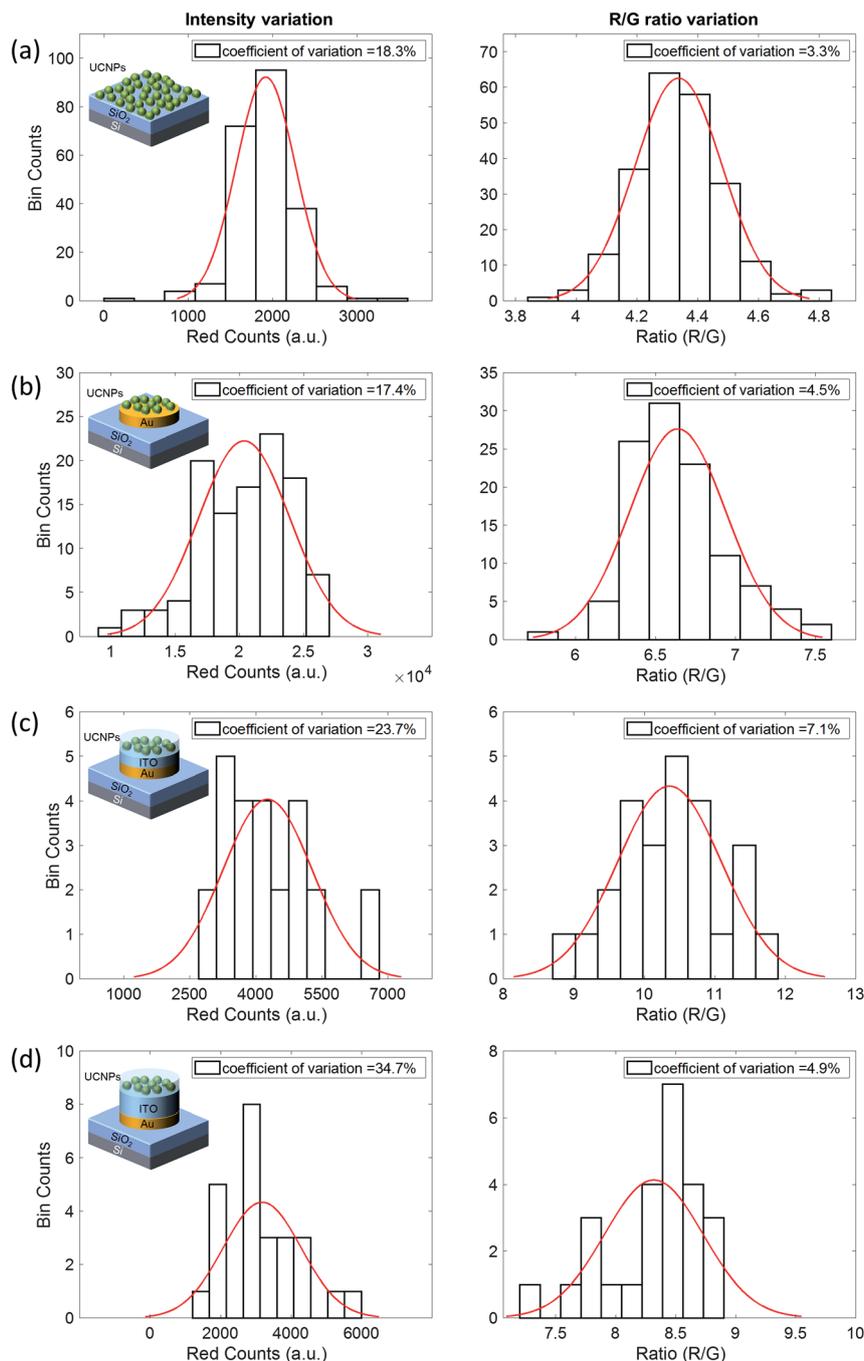
Fig. 6 Normal distribution fitting applied to the histograms of red photon counts (left column) and R/G ratio (right column) measured from UCNPs on (a) SiO$_2$ substrate, (b) Au disks without ITO, (c) Au disk with 10 nm ITO spacer layer, and (d) Au disks with 20 nm ITO spacer layer with calculated coefficients of variation.

nanodisk, we measured the PL emission from UCNPs on a larger Au nanodisk whose plasmon resonance is far away from both green and red emission bands. The Au diameter is 190 nm and the thickness is 30 nm, resulting in the plasmonic resonance at 810 nm. As shown in Fig. 5(a), the Purcell factor is nearly constant for wavelengths shorter than 700 nm and thus little changes in R/G ratio are expected from this nanostructure. The measure PL intensities confirmed this, as shown in

Fig. 5(b). The measured R/G ratios were 5.4 and 4.4 for the samples with and without Au nanodisks, respectively. The difference was about 20%. This result confirms that the bulk absorption of Au is weak in the wavelength region of our interest and thus the changes in R/G ratio arise mostly from the plasmon resonance, which can be easily controlled by the geometry and thus allows for greater engineering degree of freedom.

Finally, we recorded the PL intensity and ratio variations over a 2 mm × 2 mm area to investigate how much the signals are affected by environmental and fabrication conditions. The PL intensity variations are due to the fabrication errors, such as variations in the Au nanodisk size and shape and the number of UCNPs on the Au/ITO nanodisk. On a SiO_2 substrate without any nanopatterns, the PL intensity variation was 18.3% (left panel of Fig. 6(a)). On Au nanodisks without the ITO spacer layer, the coefficient of variation remained essentially the same at 17.4% (left panel of Fig. 6(b)). The fact that the coefficient of variation did not change upon introduction of Au nanodisks suggests the main source of variations is the nonuniformity in the nanoparticle self-assembly process used to deposit UCNPs, not the variations in Au nanodisk size and shape. Since we used the natural drying process to deposit UCNPs, the particle numbers are not uniform over a millimeter-scale area of our sample due to the formation of coffee ring patterns near the edges. The observed variation of around 18% in PL intensity should thus directly correlate with the variation in the particle number per Au nanodisk. The samples with ITO spacer layer exhibited substantially higher variations, as shown in the left panels of Fig. 6(c) and (d). Based on SEM images, the variations in size of Au and ITO nanodisks were much smaller than the observed variations. Therefore, the main cause of nonuniformity is again attributed to the variations in the number of UCNPs. The ITO surface is known to be more hydrophobic than the Au surface and this must have caused larger nonuniformity during the UCNP monolayer deposition.

In contrast to the large variations in intensities, the R/G ratio variations were significantly smaller, ranging from 3% to 7%, as shown in the right panels of Fig. 6. This is due to the self-calibration effect of ratiometric sensing. The green reference intensity is affected in the same way as the red signal intensity by the variations in the number of UCNPs. Thus, when taking the R/G ratio, these variations are canceled out. The remaining variations in the R/G ratios are due to the variations in UCNP location within a nanodisk and also the variations in size and shape of nanodisks. These results illustrate the key advantage of our ratiometric sensing. In order to perform any absolute measurements, intensity-based sensing requires the knowledge of the number of fluorescent probes in the sensing volume, which is difficult to measure or control. Any changes in the fluorescence properties due to the environment only make matters worse. In contrast, ratiometric sensing does not require the precise knowledge of the number or properties of fluorescent probes thanks to the self-calibration effect, allowing much more robust sensing. By incorporating a plasmonic nanostructure that selectively enhances the signal fluorescence, we can further improve the ratiometric sensing capability of UCNPs, as demonstrated in this paper.

4. Conclusions

In conclusion, we demonstrated the selective enhancement of upconversion luminescence using a plasmonic nanostructure, which provides an excellent platform for enhanced ratiometric sensing. The plasmonic nanostructure design consists of a monolayer of UCNPs deposited on an Au nanodisk with an ITO spacer layer. The lithographic fabrication technique we used allows for the design of a plasmonic nanostructure with a narrowband resonance that selectively excites only the red fluorescence while not affecting the green fluorescence of UCNPs. The resulting R/G ratio enhancement will directly translate to higher sensitivity and expanded dynamic range when applied to sensing. The maximum R/G ratio improvement was 4 times, achieved by Au nanodisks and 10 nm ITO spacer. The experimental results agreed well with the simulations which showed high Purcell factor only at the red wavelengths. In addition, the selective enhancement by the plasmonic nanostructure was further confirmed by using a larger size nanodisk which exhibited a plasmon resonance sufficiently detuned from the luminescence wavelengths and thus showed little changes in the R/G ratio. The ratiometric measurement showed a 3–7 percent variation, while the intensity variation was 17–35 percent, clearly demonstrating the advantages of ratiometric sensing. The proposed structure makes an excellent platform for upconversion based ratiometric sensing which could find applications in environmental and biological sensing.

Conflicts of interest

There are no conflicts to declare.

Acknowledgements

References

1 T. F. Schulze and T. W. Schmidt, *Energy Environ. Sci.*, 2015, **8**, 103–125.
2 J. C. Goldschmidt and S. Fischer, *Adv. Opt. Mater.*, 2015, **3**, 510–535.
3 Y. Il Park, K. T. Lee, Y. D. Suh and T. Hyeon, *Chem. Soc. Rev.*, 2015, **44**, 1302–1317.
4 M. Lin, Y. Zhao, S. Wang, M. Liu, Z. Duan, Y. Chen, F. Li, F. Xu and T. Lu, *Biotechnol. Adv.*, 2012, **30**, 1551–1561.
5 K. M. Mayer and J. H. Hafner, *Chem. Rev.*, 2011, **111**, 3828–3857.
6 H. Wang, T. B. Huff, D. A. Zweifel, W. He, P. S. Low, A. Wei and J.-X. Cheng, *Proc. Natl. Acad. Sci. U. S. A.*, 2005, **102**, 15752–15756.
7 P. Yuan, Y. H. Lee, M. K. Gnanasammandhan, Z. Guan, Y. Zhang and Q.-H. Xu, *Nanoscale*, 2012, **4**, 5132–5137.
8 A. Das, C. Mao, S. Cho, K. Kim and W. Park, *Nat. Commun.*, 2018, **9**, 4828.
9 J. Rieffel, F. Chen, J. Kim, G. Chen, W. Shao, S. Shao, U. Chitgupi, R. Hernandez, S. A. Graves, R. J. Nickles, P. N. Prasad, C. Kim, W. Cai and J. F. Lovell, *Adv. Mater.*, 2015, **27**, 1785–1790.
10 R. Ince and R. Narayanaswamy, *Anal. Chim. Acta*, 2006, **569**, 1–20.

11 K. Aslan and C. D. Geddes, *Anal. Chem.*, 2009, **81**, 6913–6922.

12 R. Deng, X. Xie, M. Vendrell, Y.-T. Chang and X. Liu, *J. Am. Chem. Soc.*, 2011, **133**, 20168–20171.

13 P. Huang, W. Zheng, S. Zhou, D. Tu, Z. Chen, H. Zhu, R. Li, E. Ma, M. Huang and X. Chen, *Angew. Chem. Int. Ed.*, 2014, **53**, 1252–1257.

14 L. Zhou, R. Wang, C. Yao, X. Li, C. Wang, X. Zhang, C. Xu, A. Zeng, D. Zhao and F. Zhang, *Nat. Commun.*, 2015, **6**, 6938.

15 W. Park, D. Lu and S. Ahn, *Chem. Soc. Rev.*, 2015, **44**, 2940–2962.

16 A. Das, K. Bae and W. Park, *Nanophotonics*, 2020, **9**, 1359–1371.

17 C. R. Ronda, *Luminescence: From Theory to Applications*, Weinheim, 2008.

18 E.-J. Jo, H. Mun and M.-G. Kim, *Anal. Chem.*, 2016, **88**, 2742–2746.

19 S. Wu, N. Duan, X. Ma, Y. Xia, H. Wang, Z. Wang and Q. Zhang, *Anal. Chem.*, 2012, **84**, 6263–6270.

20 Z. Li, T. Liang, S. Lv, Q. Zhuang and Z. Liu, *J. Am. Chem. Soc.*, 2015, **137**, 11179–11185.

21 M. Kumar and P. Zhang, *Langmuir*, 2009, **25**, 6024–6027.

22 P. Zhang, S. Rogelj, K. Nguyen and D. Wheeler, *J. Am. Chem. Soc.*, 2006, **128**, 12410–12411.

23 P. Alonso-Cristobal, P. Vilela, A. El-Sagheer, E. Lopez-Cabarcos, T. Brown, O. L. Muskens, J. Rubio-Retama and A. G. Kanaras, *ACS Appl. Mater. Interfaces*, 2015, **7**, 12422–12429.

24 L. Zhao, J. Peng, M. Chen, Y. Liu, L. Yao, W. Feng and F. Li, *ACS Appl. Mater. Interfaces*, 2014, **6**, 11190–11197.

25 J. Zhang, B. Li, L. Zhang and H. Jiang, *Chem. Commun.*, 2012, **48**, 4860–4862.

26 R. Wei, Z. Wei, L. Sun, J. Z. Zhang, J. Liu, X. Ge and L. Shi, *ACS Appl. Mater. Interfaces*, 2016, **8**, 400–410.

27 Z. Li and Y. Zhang, *Nanotechnology*, 2008, **19**, 345606.

28 F. Wang, Y. Han, C. S. Lim, Y. Lu, J. Wang, J. Xu, H. Chen, C. Zhang, M. Hong and X. Liu, *Nature*, 2010, **463**, 1061–1065.

29 F. Shi and Y. Zhao, *J. Mater. Chem. C*, 2014, **2**, 2198–2203.

30 N. J. J. Johnson, W. Oakden, G. J. Stanisz, R. Scott Prosser and F. C. J. M. van Veggel, *Chem. Mater.*, 2011, **23**, 3714–3722.

31 Z. Li, Y. Zhang and S. Jiang, *Adv. Mater.*, 2008, **20**, 4765–4769.

32 C. Mao, K. Min, K. Bae, S. Cho, T. Xu, H. Jeon and W. Park, *ACS Photonics*, 2019, **6**, 1882–1888.

33 J. Mei, N. Zhang and J. Friend, *JoVE*, 2020, e61013.

34 Y.-L. Wang, N. Mohammadi Estakhri, A. Johnson, H.-Y. Li, L.-X. Xu, Z. Zhang, A. Alù, Q.-Q. Wang and C.-K. (Ken) Shih, *Sci. Rep.*, 2015, **5**, 10196.

35 M. Rai, S. K. Singh, A. K. Singh, R. Prasad, B. Koch, K. Mishra and S. B. Rai, *ACS Appl. Mater. Interfaces*, 2015, **7**, 15339–15350.

36 K. Yamamoto, M. Fujii, S. Sowa, K. Imakita and K. Aoki, *J. Phys. Chem. C*, 2015, **119**, 1175–1179.

37 J. He, W. Zheng, F. Ligmajer, C.-F. Chan, Z. Bao, K.-L. Wong, X. Chen, J. Hao, J. Dai, S.-F. Yu and D. Y. Lei, *Light Sci. Appl.*, 2017, **6**, e16217.

38 S. A. Maier, *Plasmonics: Fundamentals and applications*, Springer, New York, 2007.

39 J. R. Lakowicz, *Anal. Biochem.*, 2005, **337**, 171–194.

40 M. Kang, I. Kim, M. Chu and S. W. Kim, *J. Korean Phys. Soc.*, 2011, **59**, 3280–3283.

41 Z. Wang, J. Christiansen, D. Wezendonk, X. Xie, M. A. van Huis and A. Meijerink, *Nanoscale*, 2019, **11**, 12188–12197.